

An impact of estimating tropospheric delay gradients on precise positioning in the summer using the Japanese nationwide GPS array

Shin'ichi Miyazaki,¹ Tetsuya Iwabuchi,^{2,3} Kosuke Heki,⁴ and Isao Naito⁵

Received 18 December 2000; revised 3 July 2002; accepted 17 March 2003; published 12 July 2003.

[1] We investigate the effect of modeling tropospheric delay gradients on the station position estimates using the Japanese nationwide GPS array. The time series shows spatially coherent temporal fluctuations due to the variability of water vapor distribution. This makes it difficult to identify small crustal deformation signals in GPS time series. Precision and accuracy of station positions are known to be improved by modeling the tropospheric delay gradient, and past studies suggest that delay gradient estimates agree well with the collocated water vapor radiometer measurements. Here we pick up two intervals as long as 2 weeks in 1996 summer, when remarkable tropospheric delay gradients are expected, and investigate various influences of tropospheric delay gradients on station position estimates. First, we study spatial patterns of station position deviations caused by azimuthal asymmetry of water vapor distributions from two solutions, i.e., with and without the tropospheric delay gradient model. Second, we compare them with the estimated delay gradients. Site coordinate deviations in the solution without the delay gradient model are negatively correlated with the estimated delay gradients, but such systematic deviations disappear by introducing the delay gradient model. We found that the improvement in position accuracy is significant not only horizontally but also vertically over both of the two time intervals. *INDEX TERMS*: 1243 Geodesy and Gravity: Space geodetic surveys; 1294 Geodesy and Gravity: Instruments and techniques; 0910 Exploration Geophysics: Data processing; *KEYWORDS*: GPS analysis, tropospheric delay gradient, dense GPS array, error budget in space geodesy

Citation: Miyazaki, S., T. Iwabuchi, K. Heki, and I. Naito, An impact of estimating tropospheric delay gradients on precise positioning in the summer using the Japanese nationwide GPS array, *J. Geophys. Res.*, 108(B7), 2335, doi:10.1029/2000JB000113, 2003.

1. Introduction

[2] Recent improvement of precise positioning by the Global Positioning System (GPS) has enabled us to use it for the continuous monitoring of crustal deformation. In Japan we have a large continuous GPS network, GPS Earth Observation Network (GEONET), operated by the Geographical Survey Institute (GSI) of Japan [e.g., Miyazaki *et al.*, 1996, 1997]. Although one of the main objectives of GEONET is crustal deformation monitoring, time series of site coordinates often show temporal fluctuations of up to a few centimeters on timescales of a week or so, especially in summer [e.g., Heki *et al.*, 1997, Figure 2]. Kato and Hirasawa [1999] investigated possible precursory crustal deformation signals prior to a large interplate earthquake

anticipated off the coast of central Japan by a simulation study based on rate- and state-dependent friction law, and suggested that significantly abnormal crustal deformation signals appear just before the earthquake. At the same time, they showed that the intermediate-term (a few to a few tens of days) displacements will not exceed a few centimeters, which is difficult to identify out of the time series of current accuracy of GPS measurements. It is hence important to clarify the origin of the short-term fluctuations in the time series and remove them in order to make crustal deformation monitoring by GPS practical for earthquake prediction.

[3] The spatiotemporal distribution of tropospheric water vapor is highly variable in summer over the Japanese Islands [e.g., Naito *et al.*, 1998; Iwabuchi *et al.*, 2000] and cannot be properly modeled by a mapping function assuming azimuthal symmetry of the water vapor distribution [e.g., Niell, 1996]. It is hence likely that the fluctuation in GPS time series in summer is due to the deviation of the atmosphere from this idealized state, and it is important to know how and to what extent site coordinates are affected by the unmodeled anisotropy of water vapor distribution. The tropospheric delay gradient model [e.g., MacMillan, 1995] expresses the tropospheric delay as the combination of the zenith tropospheric delay (ZTD) and an additional term to express azimuthal dependence represented by “tropospheric delay

¹Earthquake Research Institute, University of Tokyo, Tokyo, Japan.

²Japan Society for the Promotion of Science, Tokyo, Japan.

³Also at Meteorological Research Institute, Japan Meteorological Agency, Tsukuba, Japan.

⁴Division of Earth Rotation, National Astronomical Observatory, Mizusawa-city, Japan.

⁵Division of Earth Rotation, National Astronomical Observatory, Tokyo, Japan.

gradient” (we refer to it as “tropospheric gradient” or simply “gradient” hereafter). *Bar-Sever et al.* [1998] implemented the tropospheric gradient model into the GPS analysis software, GIPSY-OASIS II, and applied it to the International GPS Service (IGS) global GPS site data analysis. They first demonstrated that the gradient model improved the precision of the station position estimates in most cases. They further showed that the gradients estimated by GPS and those observed by the collocated water vapor radiometer at Onsala, Sweden, were consistent. This suggests that GPS is able to sense actual tropospheric gradients and that the station position accuracies can be improved by incorporating the gradient model in the data analysis.

[4] GEONET is dense enough to investigate the relationship between estimated gradients and meteorological conditions and the improvement of position accuracies by the gradient model. *Iwabuchi et al.* [2003] first focus on the tropospheric delays. There we investigated small but systematic differences of ZTD estimates between solutions with and without the tropospheric gradient model. These systematic ZTD differences were correlated with the north component of the tropospheric gradient [see *Iwabuchi et al.*, 2003, Figure 5]. Second, we demonstrate that the estimated gradients showed remarkable correlation with the spatial gradient of the ZTD estimated at individual stations during the weather front passage [see *Iwabuchi et al.*, 2003, Figures 7 and 8]. From these two results, we suggest that the estimated tropospheric gradients reflect real weather conditions and the ZTD estimates are improved by using the gradient model.

[5] In the present paper we discuss the fluctuation found in the position time series and the implication of the tropospheric gradient model in estimating site positions. First, we examine the spatial pattern of the fluctuations in the position time series of GSI’s network solution. Second, we investigate the correlation between the fluctuation pattern and the estimated gradients. Finally, we apply the gradient model to GEONET data to evaluate its impact on the position accuracies.

2. Drifts in GSI’s Network Solution

2.1. Outline of GEONET

[6] GSI launched the nationwide GPS array project in 1994. The first generation sites started observation in South Kanto and Tokai district (COSMOS-G2, Continuous Strain Monitoring Observation System with GPS by GSI) in April 1994 [e.g., *Sagiya et al.*, 1995] and in the whole nation (GRAPES, GPS regional array for precise surveying) in October 1994 [e.g., *Miyazaki et al.*, 1996]. The number of sites became 610 in April 1996 [*Miyazaki et al.*, 1997], and 276 and 60 sites were added in June 1997 and April 1998, respectively. The two primary objectives of GEONET are crustal deformation monitoring and the establishment of a precise active controlling point network for surveying. For the second requirement the stations are distributed as uniformly as possible (the average spacing is 25–30 km) except for a few areas especially densified for earthquake studies. The antenna-receiver types are different for each generation; Trimble 4000SSE in the COSMOS-G2 sites, Ashtech Z12 for the GRAPES sites, and Trimble 4000SSi and Leica SR9600 for later generations. The sampling rate is 30 s, and the elevation cutoff angle is 15°. The details of

the network configuration and the strategy of the routine analysis are documented by *Miyazaki et al.* [1997].

2.2. Network Solution Used in GSI’s Routine Analysis

[7] Here we briefly describe the outline of the data analysis procedure used in 1996. (The analysis strategy was improved later as described by *Hatanaka et al.* [2003].) Then GEONET consisted of 610 sites, which can be divided into three subnetworks based on their antenna-receiver types; about 110 sites of Trimble 4000SSE, about 100 sites of Ashtech Z-XIII, and about 400 sites of Trimble 4000SSi. Since there are too many stations to process as one network, an efficient analysis strategy is adopted to process the whole network as quickly as possible by dividing it into several subordinates and combining them at the final stage. First, the network is divided into two subnetworks based on the antenna-receiver types (Trimble and Ashtech networks; see *Iwabuchi et al.* [2000, Figure 8] for the subnetwork configuration). Since there are still as many as 510 stations in the Trimble subnetwork, this subnetwork is further divided into regional clusters. They are combined through a “backbone” cluster which consists of stations representing individual regional clusters. The backbone cluster is sparse but spans the whole nation in order to obtain absolute ZTD estimates as accurately as possible [*Rocken et al.*, 1993]. The Ashtech subnetwork consists of about 100 sites and is not further divided. These two subnetworks are processed independently (i.e., there are no common sites) in order to keep the antenna-receiver type homogeneous within the subnetworks. Instead, there are two Tsukuba stations within 100 m range which belong to the Trimble and Ashtech subnetworks. Their positions have been precisely determined relative to the Tsukuba International GPS Service for Geodynamics (IGS) station (TSKB) in the International Terrestrial Reference Frame (ITRF), and it is possible to obtain the consistent solution by tightly constraining the positions of those two Tsukuba stations to their a priori values. It should be noted that the two subnetworks are not correlated, and so they may have different translation/rotation errors from each other.

[8] The Bernese software version 4.1 β is used in the routine processing [*Rothacher and Marvert*, 1996]. The precise orbit information and the Earth rotation parameters provided by IGS are used, and these values are all fixed to the a priori values. The IGS_01 antenna phase map was used. ZTD parameters are estimated for every 3 hour interval. For the Trimble subnetwork ZTD’s are estimated when each regional cluster is combined with the backbone cluster, and then the station position parameters are estimated by tightly constraining the Tsukuba station. For the ZTD modeling, a simple isotropic mapping function is used as the wet mapping function:

$$M(\theta) = \frac{1}{\sin \theta}, \quad (1)$$

where θ is the satellite elevation angle. (For the dry mapping function, *Saastamoinen’s* [1972] model is used.) The essence of the analysis strategy is summarized in Table 1.

2.3. Definition of Position and ZTD Anomalies

[9] Our main concern is to study the influence of anisotropic distributions of water vapor on the position estimates.

Table 1. Analysis Strategy of GSI's Network Solution (Net), No-Gradient Point Solution (No-grad), and Gradient Point Solution (Grad)^a

Strategy	Mapping Function	Orbit	Ocean Loading	ZTD Estimation		Gradient Estimation	
				Method	Interval	Method	Interval
Net	1/sin(θ)	IGS	no	deterministic	3 hours	no	—
Grad	Niell [1996]	JPL ^b	GOTIC2 ^c	stochastic ^d	5 min	no	—
No-grad	Niell [1996]	JPL ^b	GOTIC2 ^c	stochastic ^d	5 min	stochastic ^e	5 min

^aThe satellite elevation cutoff angle is 15° for all solutions.

^bPrecise fiducial-free orbit and transformation parameter provided by JPL.

^cMatsumoto *et al.* [2001].

^dRandom walk with $\tau = 5.0 \times 10^{-8}$ km/ \sqrt{s} .

^eRandom walk with $\tau = 5.0 \times 10^{-9}$ km/ \sqrt{s} .

Here we define measures useful to characterize the influence. Besides troposphere variations, errors in the reference frame realization give rise to short-term noises in GPS time series. In the present study we adopt the following strategy to isolate the position errors of atmospheric origin. The reference frame errors affect solutions through global parameters such as satellite ephemerides and the fiducial site positions and can be modeled by the seven parameter transformation of the network (translation, rotation, and scale adjustments). For local or regional networks it is usually sufficient to apply only a translation to realize the frame in local or regional scales [e.g., *Wdowinski et al.*, 1997]. As this kind of frame we adopt the “zero-mean” frame to be established as follows: (1) we calculate the daily deviations of the position of each station from the average (crustal deformation is negligible in a short period),

$$\Delta\mathbf{X}(\mathbf{r}, t) = \mathbf{X}(\mathbf{r}, t) - \overline{\mathbf{X}(\mathbf{r}, t)} \quad (2)$$

$$\text{Var}(\mathbf{r}) = \overline{\Delta\mathbf{X}(\mathbf{r}, t)^2}, \quad (3)$$

where $\overline{\mathbf{X}(\mathbf{r}, t)}$ and $\text{Var}(\mathbf{r})$ represent a temporal average of position estimates at a site and a variance of position estimates at a site, respectively; (2) we apply a translation at each epoch:

$$\Delta\mathbf{x}(\mathbf{r}, t) = \Delta\mathbf{X}(\mathbf{r}, t) - \langle \Delta\mathbf{X}(\mathbf{r}, t) \rangle, \quad (4)$$

$$\text{Var}(t) = \langle \Delta\mathbf{x}(\mathbf{r}, t)^2 \rangle, \quad (5)$$

where the angle brackets represent a spatial average from all observation stations and $\text{Var}(t)$ represents a variance of position estimates from all sites at a given epoch. We refer to $\Delta\mathbf{x}(\mathbf{r}, t)$ as “position anomaly.” Errors due to the global parameters are mostly removed by this procedure, and the remaining position anomalies represent either site dependent monument instabilities or apparent displacements caused by atmosphere. Above all, spatially coherent errors are likely to reflect anisotropic water vapor distribution.

[10] Similarly, by subtracting the ZTD averaged over the period for each station, we express temporal fluctuations of the zenith wet delay component as

$$\Delta ZTD(\mathbf{r}, t) = ZTD(\mathbf{r}, t) - \overline{ZTD(\mathbf{r}, t)}. \quad (6)$$

Because the zenith hydrostatic delays and steady components of the zenith wet delay of each site are included in $\overline{ZTD(\mathbf{r}, t)}$, we call $\Delta ZTD(\mathbf{r}, t)$ the “ZTD anomaly.”

2.4. Weather and GPS Data

[11] In the present study, we focus on two periods in summer: period A is 16–29 July 1996 (the end of the rainy season), and period B is 28 August to 10 September 1996 (the end of summer). We used 14 days of data for each period, which is appropriate to characterize the weather conditions in Japan that are quite variable in summer. Those periods include meteorological phenomena that might have caused remarkable azimuth dependency of the water vapor distribution. We selected the following two phenomena from the two periods (Figure 1): in case a, a tropical cyclone stayed over central Japan on 20 July, and in case b, a weather front passed over the Japanese Islands on 1 September. By studying position anomalies on those days, we will investigate their relationship with the tropospheric gradient. We excluded outlier data larger than 3 times the ensemble standard deviation and excluded stations where data were collected for <11 days.

2.5. A Relationship Between Position and ZTD Anomalies

[12] We calculated the position and ZTD anomalies for periods A and B. Since positions are estimated daily, we compared daily averages of the ZTD anomalies with the position anomalies of the same days. As seen in Figure 2, position anomalies tend to be large where ZTD anomalies have large spatial gradients, and to be directed perpendicular to the ZTD anomaly contours toward local minima. This pattern is remarkable around the tropical cyclone in Figure 2a and the weather front in Figure 2b. This suggests a close relationship between the position anomaly and the spatial gradient of ZTD anomalies and that a certain portion of GPS site position errors is caused by anisotropic water vapor distributions [*Tsuda et al.*, 1998].

[13] We can also see that some stations have significant position biases. By comparing the examples (Figure 2b) with the receiver-antenna types deployed in GEONET [see *Iwabuchi et al.*, 2000, Figure 8], we found that the biases are observed only at sites with Ashtech receivers/antennas. This is due partly to the data analysis strategy described above. Although Figure 2 strongly suggests a close relationship between the position and ZTD anomalies, such a bias suggests that the GSI's network solution is inappropriate for further discussions. In section 3, we reprocess the

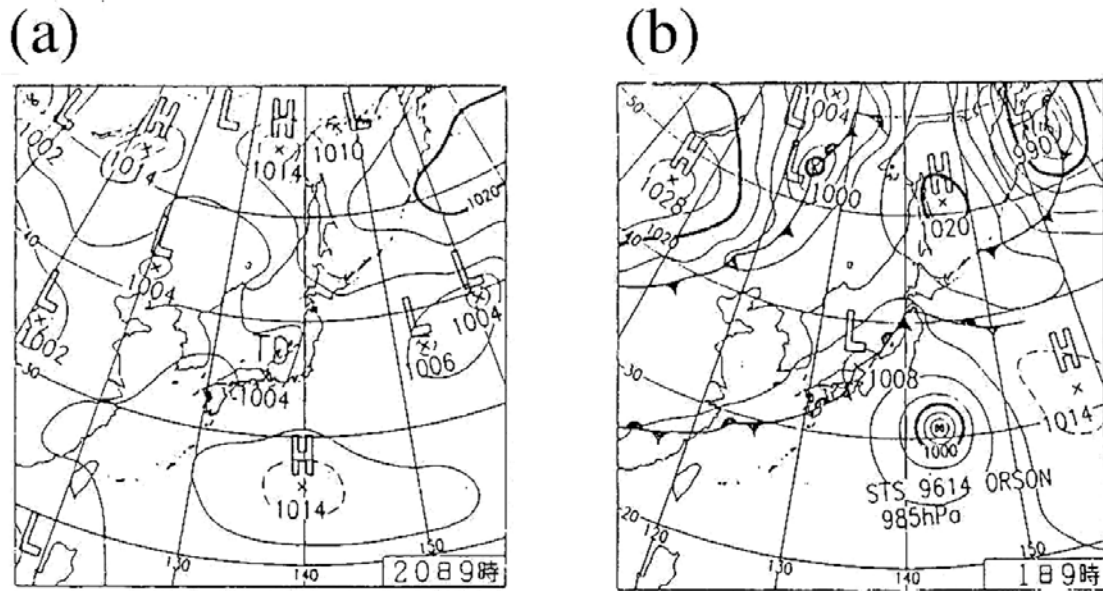


Figure 1. Weather map at 0000 UT on (a) 20 July and (b) 1 September 1996 (courtesy of the Japan Meteorological Agency). The maps show a tropical cyclone off central Japan on 20 July, and a weather front that moved eastward over the Japanese Islands on 1 September.

same data sets with a precise point positioning strategy [Zumberge *et al.*, 1997].

3. Effects of Tropospheric Gradient Model

3.1. Data Analysis Model

[14] Systematic errors due to anisotropic water vapor distributions would be reduced by using more realistic

tropospheric mapping functions, i.e., to represent azimuthally dependent delay components by tropospheric delay gradients. The gradient model was first successfully applied in very long baseline interferometry (VLBI) analyses by *Herring* [1992] and *MacMillan* [1995]. *MacMillan* [1995] modeled the contribution of tropospheric gradients ΔD to delay as

$$\Delta D = M(\theta) \cot\theta [G_E \sin\phi + G_N \cos\phi], \quad (7)$$

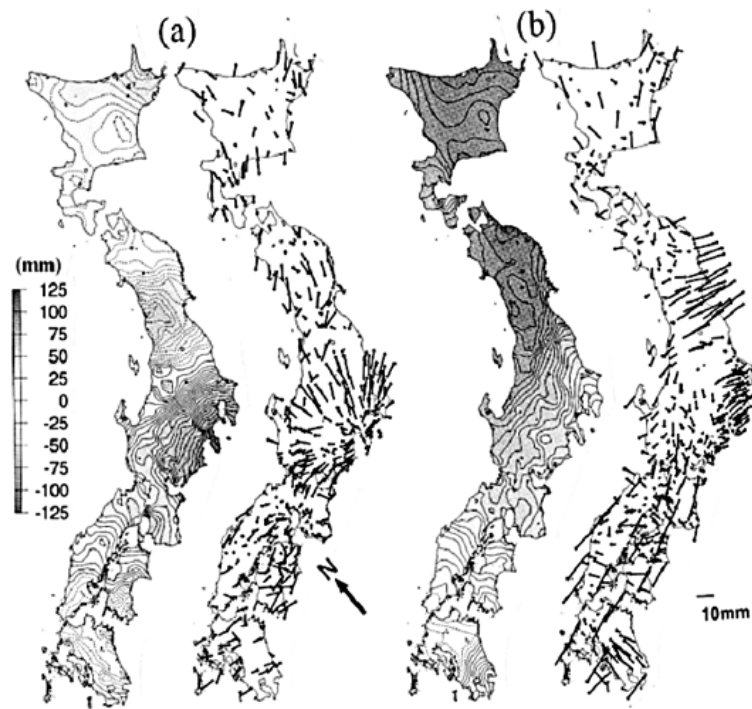


Figure 2. Spatial distribution of the “zenith tropospheric delay (ZTD) anomaly” and the “position anomaly” retrieved from the network solution for (a) case a and (b) case b, respectively.

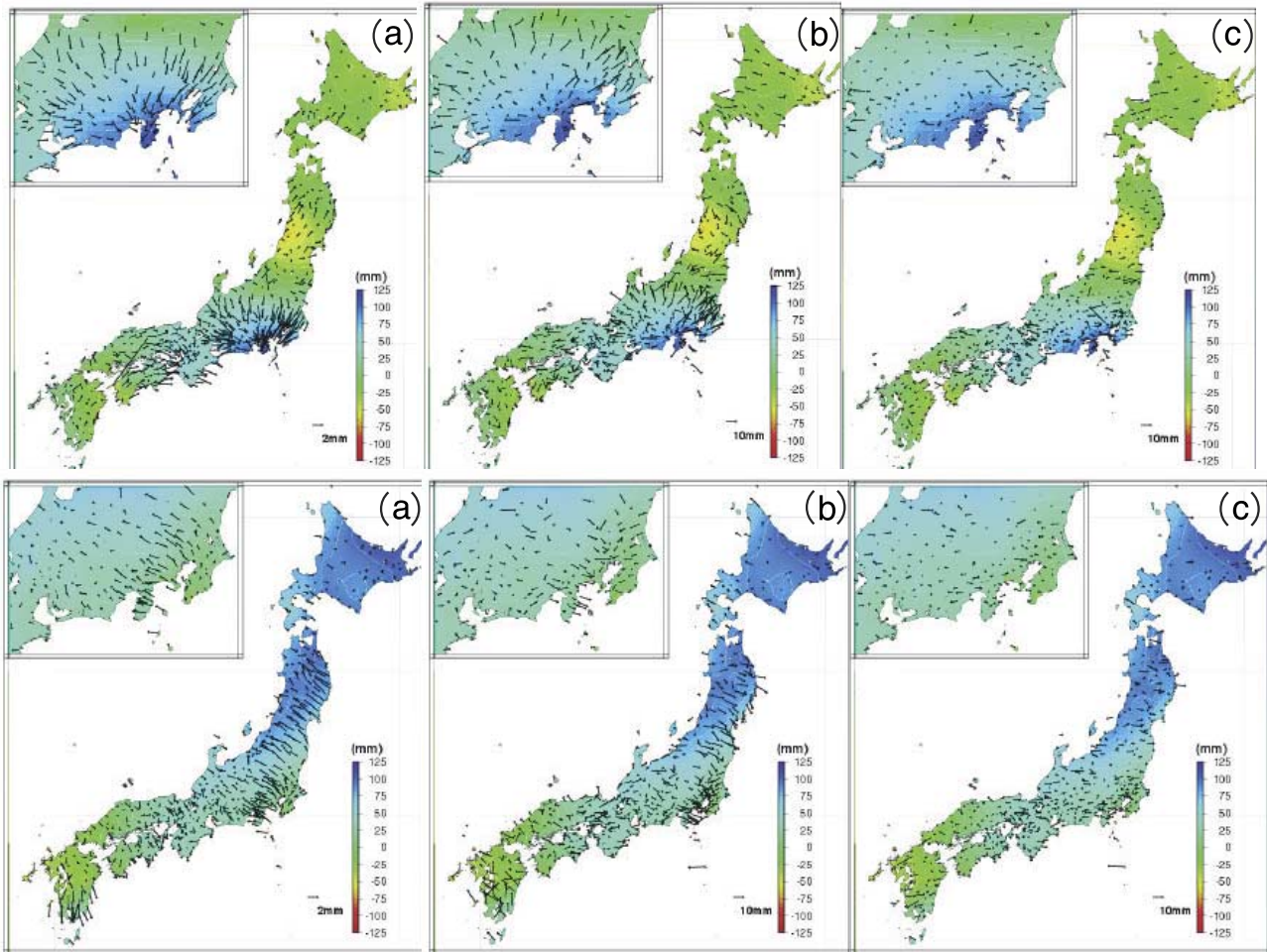


Figure 3. Spatial distribution of the zenith tropospheric delay (ZTD) anomaly, the tropospheric gradient anomaly, and the horizontal position anomalies for cases (top) a and (bottom) b. The inset shows a detailed plot for the region around Tokyo. (a) Gradient vector anomalies superimposed on the ZTD anomaly (corresponding to the right color bar scale). The gradient anomalies are mostly perpendicular to the ZTD anomaly contour lines toward the local maxima. (b and c) Horizontal position anomalies for the no-gradient point solution and gradient point solution, respectively, superimposed on the ZTD anomaly. The horizontal position anomalies for the no-gradient point solution are perpendicular to the ZTD anomaly contour lines toward the local minima and show the negative correlation with the tropospheric gradient anomalies. Such a systematic pattern of the gradient anomaly disappear in the gradient solution.

where ϕ is the azimuth measured clockwise from north, θ is the elevation, and $M(\theta)$ is the isotropic mapping function that depends only on the elevation angle. $\mathbf{G} = (G_N, G_E)$ is the “gradient vector” that represents the magnitude and direction of the tropospheric delay anisotropy (see *Davis et al.* [1993] for the derivation and the physical meaning of the gradient vector). *MacMillan* [1995] showed that the position repeatability was significantly improved by using the gradient model. Similar results were reported for VLBI data by *Chen and Herring* [1997], who employed a more accurate gradient model, especially at low elevation angles.

[15] Similar efforts have also been made in GPS data analyses. *Bar-Sever et al.* [1998] implemented *MacMillan*’s [1995] gradient model in GIPSY-OASIS II software and demonstrated that the model improved the repeatability in precise point positioning. On the basis of extensive point positioning experiments, they concluded that the best strat-

egy is to use the elevation cutoff of 7° and to model the variation of tropospheric gradients as a random walk process (5.0×10^{-9} km/ \sqrt{s}). From direct comparisons between data from GPS and a collocated WVR, they further suggested that the GPS solution seemed to well reproduce the variation of the wet gradient component over timescales as short as 15 min. These conclusions suggest that the gradient model would significantly improve both of the accuracy and precision of position estimates.

[16] We introduce the “tropospheric gradient anomalies” to represent temporal fluctuations of gradients (wet component) to be calculated similarly to the ZTD anomalies. We use GIPSY-OASIS II software release 2.6 and employ the precise point positioning strategy, which does not have the subnetwork concept, to investigate relationships among the position anomaly, the ZTD anomaly, and the tropospheric gradient anomaly in the cases a and b. For this purpose we perform

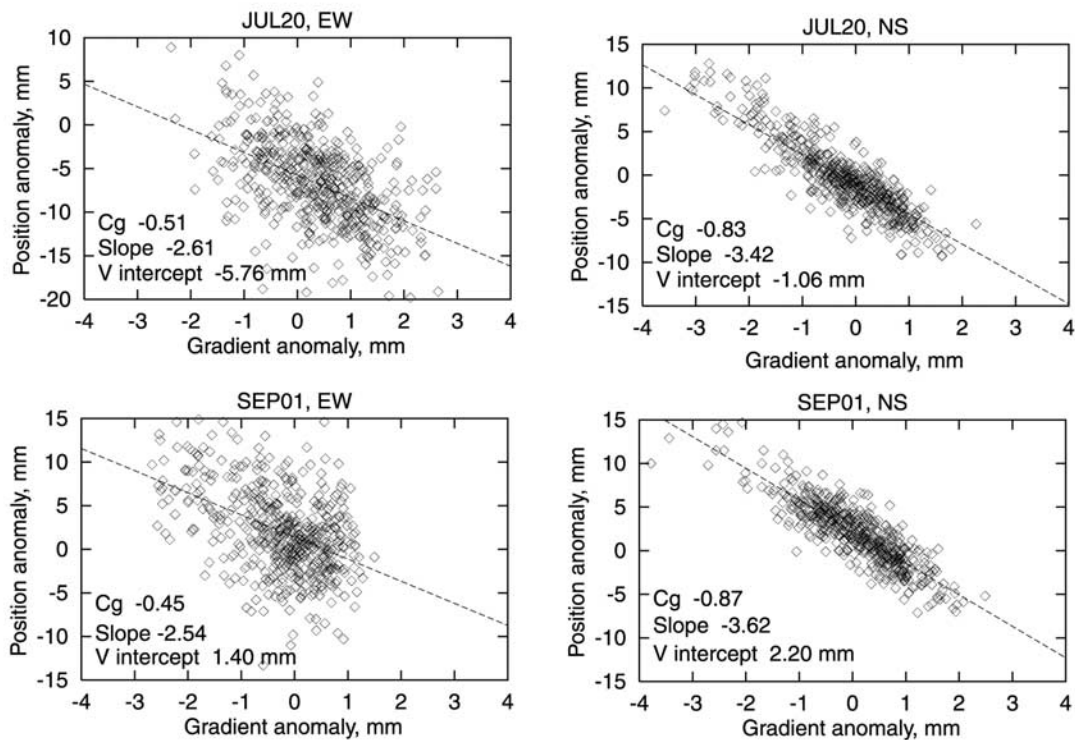


Figure 4. Scatter diagram for the position anomaly of (left) east component and (right) north component for the no-gradient point solution and the tropospheric gradient anomaly of the gradient point solution for cases (top) a and (bottom) b, respectively. The vertical and horizontal axes show the position anomaly and the gradient anomaly, respectively. The result of the linear regression and the correlation coefficients (Cg) are displayed.

precise point positioning analyses with and without the tropospheric gradient model and refer to the solutions as the “gradient point solution” and the “no-gradient point solution,” respectively. When gradients are estimated from GPS data, it is possible that gradient effects are correlated with antenna phase center variations and with multipath effects. A model of antennal phase center variations has recently been improved by *Hatanaka et al.* [2001a, 2001b] for GEONET stations. We use their new antenna phase center variation model in both analyses to isolate the tropospheric gradients, together with Niell’s mapping function [*Niell, 1996*] for the isotropic delay and an ocean tidal loading correction calculated by GOTIC2 [*Matsumoto et al., 2001*]. The initial values for ZTD and tropospheric gradient are set to 50 cm and 0 cm, respectively, and both quantities are modeled to vary according to random walk processes with the scale parameters 5.0×10^{-8} km/ \sqrt{s} ($= 3.0$ mm/ \sqrt{h}) and 5.0×10^{-9} km/ \sqrt{s} ($= 0.3$ mm/ \sqrt{h}), respectively, following *Bar-Sever et al.* [1998]. Both are estimated at 5 min intervals. We use precise fiducial free orbits, satellite clocks, and transformation parameters that relate the fiducial free system to ITRF97, provided by the Jet Propulsion Laboratory (JPL), and we estimate daily station positions. The minimum elevation angle is set to 15° since lower elevation data than 15° are not available in GEONET. The analysis strategy is summarized in Table 1.

[17] We calculate both vertical and horizontal components of position anomalies to investigate the influence of tropo-

spheric gradients. In the present paper we compare daily averages of ZTD and tropospheric gradient anomalies with daily position anomalies. Behaviors of tropospheric delays in short-term periods are discussed by *Iwabuchi et al.* [2003].

3.2. Gradient Anomaly and Position Anomaly of No-Gradient Point Solution

[18] As summarized in Appendix A, tropospheric gradient anomalies and position anomalies should be closely related. In this section we study this relationship in the actual results of GPS analyses. In Figure 3 we show the tropospheric gradient anomaly superimposed on the ZTD anomaly for cases a and b in Figure 3a. Similarly, the horizontal position anomalies for the no-gradient and gradient point solutions are shown in Figures 3b and 3c. The gradient anomalies are generally perpendicular to the ZTD anomaly contour lines. The horizontal position anomaly vectors for the no-gradient point solution are also perpendicular to the ZTD anomaly contour lines and show the negative correlation with the tropospheric gradient anomalies. Those results suggest that the horizontal position anomalies in the no-gradient solution is caused by the anisotropic water vapor distribution in the tropical cyclone and in the weather front and the tropospheric gradient anomaly actually represents the anisotropic water vapor distributions.

[19] Tropospheric gradients and horizontal position anomalies have the following relationship under the full

satellite coverage of the minimum elevation angle of $\theta \geq 15^\circ$ and the azimuth $40^\circ \leq \phi \leq 320^\circ$ (Appendix A),

$$\begin{aligned}
 \Delta \mathbf{x}_E(\mathbf{r}, t) &= A_E \mathbf{G}_E(\mathbf{r}, t) \\
 &= -5.1 \mathbf{G}_E(\mathbf{r}, t) \\
 \Delta \mathbf{x}_N(\mathbf{r}, t) &= A_N \mathbf{G}_N(\mathbf{r}, t) \\
 &= -6.3 \mathbf{G}_N(\mathbf{r}, t) \\
 \Delta \mathbf{x}_U(\mathbf{r}, t) &= A_U \mathbf{G}_U(\mathbf{r}, t) \\
 &= 2.4 \mathbf{G}_U(\mathbf{r}, t).
 \end{aligned} \tag{8}$$

If $\mathbf{G}(t)$ in equation (8) is the tropospheric gradient anomaly, $\Delta \mathbf{x}(\mathbf{r}, t)$ would represent the horizontal position anomaly. We show correlations between the position and the gradient anomalies in Figure 4 for the north and east components. It should be noted that we used only stations near the tropical cyclone for case a and near the weather front for case b (see *Iwabuchi et al.* [2003, Figure 8] for the selected stations). For case a, A_E and A_N have values of -2.6 and -3.4 , and the correlation coefficients are -0.51 and -0.83 , respectively. For case b, A_E and A_N are -2.5 and -3.6 , and the correlation coefficients are -0.45 and -0.87 , respectively. Those A factors are smaller than the predicted values shown in equation (8) because of the difference of path delays between the one that a simple gradient model gives and the other that an actual meteorological condition gives, especially at low elevation angles. *Iwabuchi et al.* [2003] demonstrated that the tropospheric gradient anomaly obtained by GPS has a correlation with grad $[\Delta ZTD(t)]$ as high as 0.94 in case b, suggesting the physical reality of the estimated gradient anomaly. These results indicate that the horizontal position anomaly in the no-gradient point solution is due mainly to the anisotropic water vapor distribution.

[20] The correlation between the position anomaly of the no-gradient point solution and the gradient anomaly is weaker in the east component than the north. Weather changes from west to east over the Japanese Islands. *Iwabuchi et al.* [2003] detected rapid temporal changes of the ZTD and tropospheric gradient distribution for case b. They showed that it took <12 hours for the weather front to pass across northeast Japan and that the gradient changed its direction when the front passed over the stations. The present study uses daily averages of ZTD and the gradient anomalies, and this operation might have cancelled out these short-term anomalies and degraded the correlation in the east component.

3.3. Improvement of Position Estimates

[21] Systematic patterns found in the position anomalies of the no-gradient point solution is absent in the gradient solution (Figure 3). There still remain random components in the position anomalies due possibly to a local water vapor irregularities as large as a few kilometers [*Shimada et al.*, 2002], but the larger-scale water vapor distributions seem to be modeled by gradient parameters to a large extent. We calculate the standard deviation of position anomalies for the no-gradient and gradient solutions for cases a and b and

Table 2. Root-Mean-Square Scatter of the Position Estimates for North (N), East (E) and Vertical (U) Components at Each Epoch^a

	Number of Sites	RMS (NG, NEU), mm			RMS (G, NEU), mm		
		North	East	Vertical	North	East	Vertical
<i>Period A</i>							
16 July 1996	529	3.06	3.93	8.02	2.11	3.58	7.81
17 July 1996	532	4.92	4.66	9.80	2.39	3.92	9.04
18 July 1996	520	3.90	5.01	10.08	2.67	3.88	9.31
19 July 1996	459	4.06	5.10	8.33	2.25	4.10	7.69
20 July 1996	534	4.07	4.76	7.86	1.94	3.75	7.15
21 July 1996	533	3.01	5.06	7.11	1.86	3.95	6.58
22 July 1996	525	2.49	4.23	7.52	1.86	3.38	7.00
23 July 1996	518	3.89	4.80	8.71	1.95	3.81	7.82
24 July 1996	531	2.78	4.35	7.50	2.17	3.94	7.68
25 July 1996	534	2.90	4.36	7.43	1.99	3.38	6.80
26 July 1996	456	2.94	4.36	8.46	2.09	3.80	8.45
27 July 1996	531	3.39	4.39	8.44	1.90	3.86	7.98
28 July 1996	515	3.78	4.94	7.89	2.08	4.65	6.60
29 July 1996	506	3.82	4.78	8.14	2.83	4.22	7.28
Total/means	7223	3.56	4.63	8.27	2.17	3.88	7.69
<i>Period B</i>							
28 Aug. 1996	523	3.93	4.40	9.76	2.16	4.15	9.28
29 Aug. 1996	532	3.37	4.16	7.85	1.74	3.49	7.11
30 Aug. 1996	478	4.45	4.12	9.64	2.03	4.13	9.61
31 Aug. 1996	530	4.34	4.37	8.72	1.91	3.55	7.79
1 Sept. 1996	533	3.68	4.79	10.05	1.82	3.75	8.67
2 Sept. 1996	531	3.83	4.78	8.36	2.16	4.76	7.77
3 Sept. 1996	527	2.96	4.00	8.90	1.60	3.64	9.03
4 Sept. 1996	537	3.39	4.26	8.22	1.75	4.07	7.48
5 Sept. 1996	532	3.27	4.47	9.12	1.85	4.20	8.78
6 Sept. 1996	539	3.92	4.11	11.32	2.22	3.90	9.88
7 Sept. 1996	499	3.81	3.99	7.54	1.77	3.82	6.38
8 Sept. 1996	542	2.80	3.36	7.87	1.80	3.15	7.05
9 Sept. 1996	540	3.57	3.96	8.72	1.90	3.45	8.43
10 Sept. 1996	539	3.70	3.99	8.45	1.82	3.51	7.78
Total or mean	7382	3.66	4.21	8.95	1.90	3.84	8.27

^aThat is, square root of equation (4) for no-gradient point solution (NG) and gradient point solution (G).

summarize the results in Table 2. We plot the difference between the position anomalies in the gradient and the no-gradient point solutions for north, east, and vertical components in Figure 5 and call them “position anomaly difference” hereafter.

[22] First, we recognize strong correlation between the position anomaly differences in the horizontal components and the weather conditions (Figure 1). As described above, the anomaly difference is positive where the gradient anomaly is northward or eastward, and this correlation is stronger “around” the weather front or the tropical cyclone where the anisotropic part is modeled fairly well by the simple gradient model. The anomaly difference reaches ~ 10 mm there. On the contrary, just “above” the tropical cyclone or the weather front, water vapor is distributed in a more complex manner.

[23] Second, we can also see that the vertical components of the anomaly difference show quite similar spatial patterns with the horizontal components, especially with the north component. With an analytical approach presented in Appendix A, we demonstrate that the presence of northward tropospheric gradient causes a position anomaly not only in north component but also in the vertical component, as we have shown in equation (8).

[24] We further investigated this by analyzing data simulated using GPSSIM, one of the programs (source code was slightly modified to enable applications of tropospheric

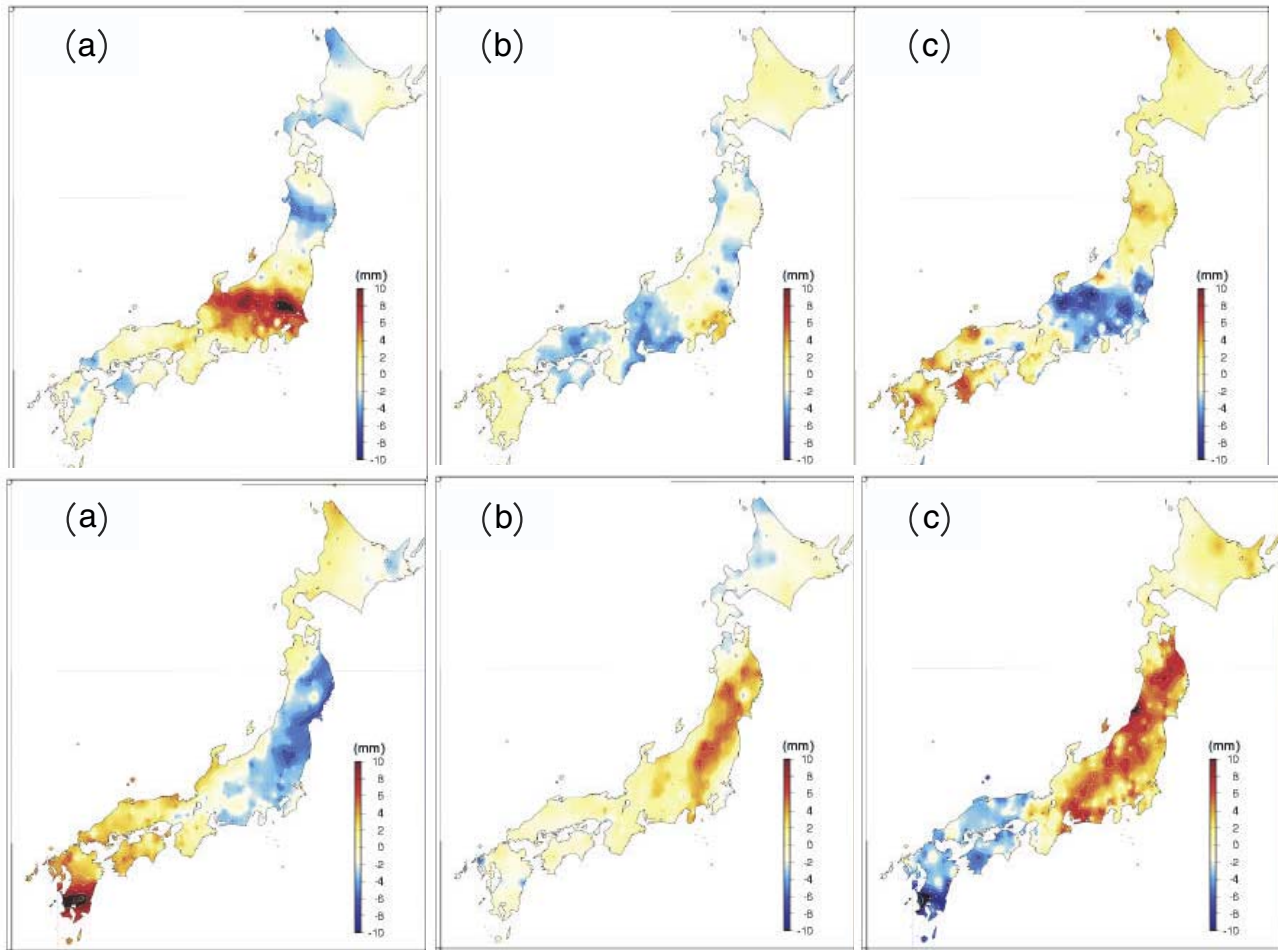


Figure 5. Spatial distribution of the position anomaly differences between the gradient and no-gradient point solutions for (top) case a and (bottom) case b. Position anomaly difference is defined as the difference between the position anomalies in the gradient and the no-gradient point solutions for each component. (a), (b), and (c) are north, east, and vertical components of the position anomaly difference, respectively. We recognize strong correlation between the position anomaly differences in the horizontal components and the weather conditions. We also see that the vertical components of the anomaly difference (Figure 5c) show quite similar spatial patterns with the horizontal components, especially with the north component (Figure 5a).

gradients) in the Bernese GPS software 4.0 [Rothacher and Marvert, 1996]. We assume a virtual observation site in Mizusawa, Japan, located in 39°N , and the ephemeris file on 8 March 1995, and generated 24-hour synthetic data using various elevation cutoff angles. We applied fixed amount of northward tropospheric gradient, and estimated the station position and the ZTD simultaneously as if we did not know the existence of tropospheric gradients. Figure 6 shows the ratio between the applied gradient and the shift of the position estimates, where we can see that the north tropospheric gradient affects not only the north position component but also the vertical component and ZTD estimates. Because the inclinations of the orbits of the Block II GPS satellites are set to 55°N (i.e., there are no satellites with polar orbits), there is a void in the northern (southern) sky in the satellite sky coverage when the station is in the Northern (Southern) Hemisphere. It is this north-south asymmetry in GPS satellite distribution that gives rise

to the shift in the vertical position and ZTD. The vertical position shifts are comparable in magnitude and opposite in sense to those in north. This simulation study suggests that the vertical position anomaly differences are also due to tropospheric gradients. It should be noted that it depends on the site latitude to what extent the vertical component shifts, e.g., the shift disappears on the equator and at poles where the satellite coverage is azimuthally symmetric. The effect on the ZTD estimates in the same data set is also discussed by Iwabuchi *et al.* [2003]. Thus the gradient model in GPS data analysis improves the accuracy and precision of both vertical and horizontal station positions.

[25] In addition to the daily results for cases a and b, we calculate the root-mean-square scatter (square root of equation (5)) at each observation epoch over the periods A and B for the no-gradient point solution and the gradient point solution, and summarize the results in Table 2. The standard deviation of the gradient point solution is generally smaller

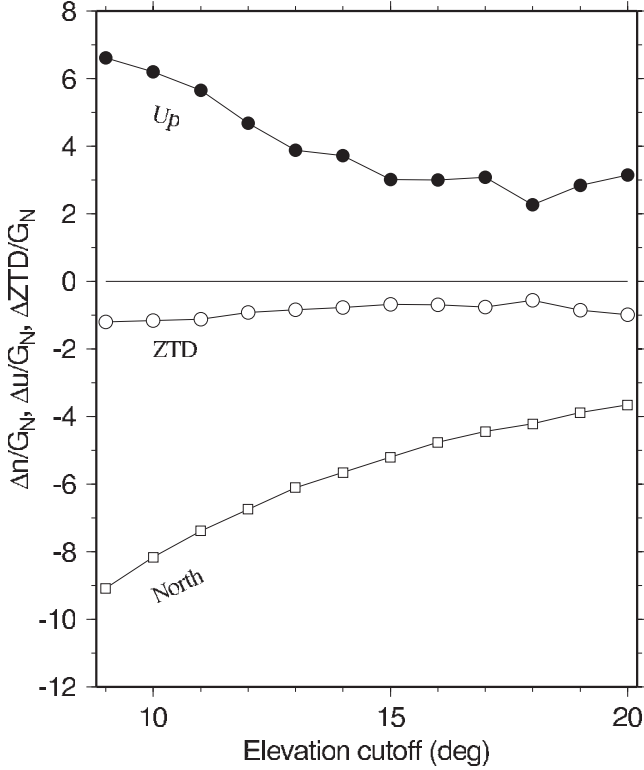


Figure 6. Simulation result of the effect of mismodeling the tropospheric gradient on the position estimates. The horizontal axis represents the satellite cutoff elevation angle and the vertical axis shows the bias from the true value as the ratio to the imposed gradient. The open rectangles, solid circles, open circles are the results for the north component, the vertical component, and the zenith delay, respectively.

than that of the no-gradient point solution at almost all epochs. Among the three components, improvement in the north component is the largest; the standard deviation was reduced by 1.5 mm on average over the periods A and B. On the other hand, that of the east was reduced by <1 mm. As already mentioned, this is likely to be due to rapid weather changes from west to east in Japan and to the averaging over one day periods. The vertical component is also improved by about 0.5 mm.

[26] Figures 7 (top) and 7 (bottom) show the change of the root-mean-square of position anomalies between the no-gradient and gradient solutions averaged over periods A and B, respectively. The improvement of the solution is remarkable “around” the weather front or the tropical cyclone. We find no region, except for several stations, where the gradient model either dramatically improved or degraded the position estimations. This result demonstrates that the gradient formulation is generally adequate to represent the atmospheric delay variations.

4. Conclusion

[27] We investigated the influences of the anisotropic water vapor distributions and the implication of the tropospheric gradient model in GPS baseline analyses. For this purpose we selected two 14 day intervals, one at the end of

the rainy season and the other at the end of summer. During the first a tropical cyclone remained off central Japan, and during the second a weather front passed across the Japanese islands.

[28] First, we extracted short-term drifts of the position estimate from the network solution by subtracting the average over the period and removing the reference frame realization errors. The remaining position anomalies were correlated with the zenith wet delay anomaly, which suggests that the position anomalies originate largely from the anisotropic water vapor distributions.

[29] Second, in order to evaluate the contribution of tropospheric gradients to the positioning, we performed two precise point positioning analyses, i.e., with and without the gradient model. Similar position anomalies were found in the no-gradient point solution, and its spatial pattern showed significant negative correlation with the estimated gradients, especially around the cyclone and the weather front. On the other hand, position errors were not systematic in the gradient point solution. The vertical components of the position anomaly differences between the gradient and the no-gradient point solutions showed negative correlation with those of north components. This is consistent with our simulation study and suggests that the gradient model improves accuracies in vertical coordinates as well as those in the horizontal plane.

Appendix A: Relationship Between Position Anomaly and Tropospheric Gradient Anomaly

[30] *Beutler et al.* [1988] studied the effects of various biases, such as troposphere, fixed station coordinates, along track orbit error, and so on, for a quasi-hemispherical satellite configuration. *Santerre* [1991] studied the effects of some important systematic errors on precise relative positioning as a function of GPS satellite sky distribution. In this appendix, we use a simple parameter model, in which only station coordinates are estimated, to derive the effect of unmodeled tropospheric gradients on estimates of position (east, north, up) using the same function of GPS satellite sky distribution as employed by *Santerre* [1991].

[31] By generalizing the formulation of *MacMillan*. [1995], the unmodeled delay due to tropospheric gradients is expressed as

$$T = -\frac{dM(\theta)}{d\theta} [G_E \sin \phi + G_N \cos \phi], \quad (\text{A1})$$

where $M(\theta)$ is a isotropic mapping function, θ is the satellite elevation angle, and ϕ is the azimuth measured clockwise from north. Here we approximate $M(\theta)$ by $1/\sin \theta$. Partial derivatives of T with respect to the station coordinates e (east), n (north), u (vertical) are

$$\begin{aligned} \frac{\partial T}{\partial e} &= \cos \theta \sin \phi, \\ \frac{\partial T}{\partial n} &= \cos \theta \cos \phi, \\ \frac{\partial T}{\partial u} &= -\sin \theta. \end{aligned} \quad (\text{A2})$$

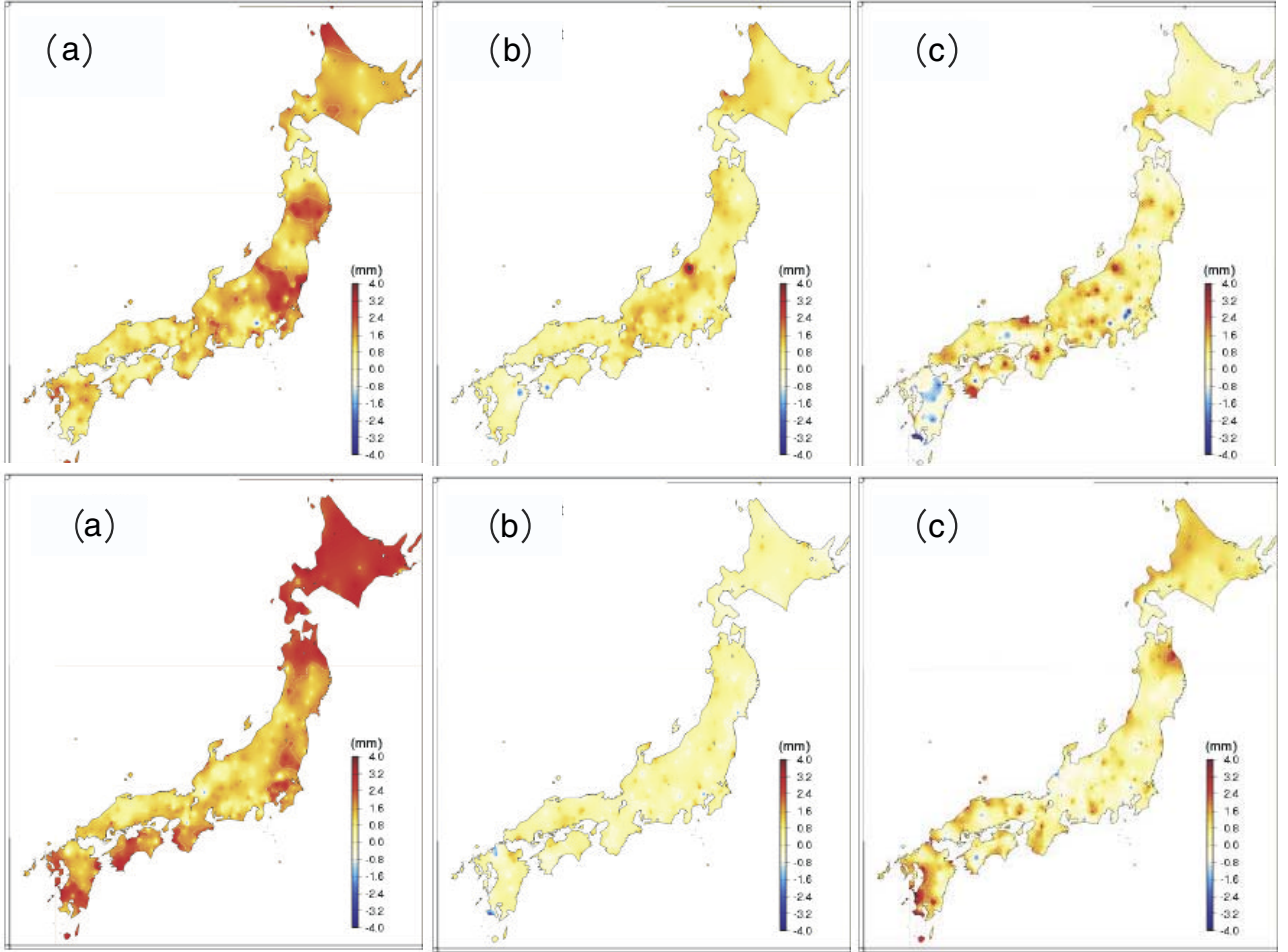


Figure 7. Spatial distribution of the root-mean-square scatter differences between the gradient and no-gradient point solutions for cases (top) a and (bottom) b. (a), (b), and (c) North, east, and vertical components of the RMS scatter differences of the no-gradient solution from the gradient solution. The improvement of the solution is remarkable “around” the weather front or the tropical cyclone. We find no region, except for several stations, where the gradient model degraded the position estimations.

If we assume that there is no error in the isotropic component of the tropospheric delay, the observation equation becomes

$$T = F\Delta\mathbf{x}, \quad (\text{A3})$$

where

$$\begin{aligned} T &= -\frac{dM(\theta)}{d\theta} [G_E \sin \phi + G_N \cos \phi], \\ F &= [\cos \theta \sin \phi, \cos \theta \cos \phi, -\sin \theta], \\ \Delta\mathbf{x} &= [\Delta\mathbf{x}_E, \Delta\mathbf{x}_N, \Delta\mathbf{x}_U]^T. \end{aligned} \quad (\text{A4})$$

Assuming that satellites fully distribute over the area of $\theta_{\min} \leq \theta \leq \pi/2$ and $\phi_c \leq \phi \leq 2\pi - \phi_c$, the normal equation is

$$N\Delta\mathbf{x} = \mathbf{B}, \quad (\text{A5})$$

where

$$\begin{aligned} N_{ij} &= \langle (F^T F)_{ij} \rangle, \\ B_i &= \langle (F^T T)_i \rangle, \end{aligned} \quad (\text{A6})$$

$$\langle \rangle = \int_{\phi_c}^{2\pi-\phi_c} d\phi \int_{\theta_m}^{\pi/2} d\theta \cos \theta.$$

Executing the integration, we obtain

$$N_{11} = \frac{1}{6} (2\pi - 2\phi_c + \sin 2\phi_c) \cdot (2 - 3 \sin \theta_m + \sin^3 \theta_m), \quad (\text{A7})$$

$$N_{12} = N_{21} = 0, \quad (\text{A8})$$

$$N_{13} = N_{31} = 0, \quad (\text{A9})$$

$$N_{22} = \frac{1}{6} (2\pi - 2\phi_c + \sin 2\phi_c) \cdot (2 - 3 \sin \theta_m + \sin^3 \theta_m), \quad (\text{A10})$$

$$N_{23} = N_{32} = \frac{2}{3} \sin \phi_c \cos^3 \theta_m, \quad (\text{A11})$$

$$N_{33} = \frac{2}{3} (\pi - \phi_c) (1 - \sin^3 \theta_m), \quad (\text{A12})$$

$$B_1 = \frac{1}{2} G_E (2\pi - 2\phi_c + \sin 2\phi_c) \cdot \left(\sin \theta_m + \frac{1}{\sin \theta_m} - 2 \right), \quad (\text{A13})$$

$$B_2 = \frac{1}{2} G_N (2\pi - 2\phi_c - \sin 2\phi_c) \cdot \left(\sin \theta_m + \frac{1}{\sin \theta_m} - 2 \right), \quad (\text{A14})$$

$$B_3 = -2G_N \sin \phi_c \left[\log \left(\tan \frac{\theta_m}{2} \right) + \cos \theta_m \right]. \quad (\text{A15})$$

It should be noted that $\Delta \mathbf{x}_E$ is decoupled but that $\Delta \mathbf{x}_N$ and $\Delta \mathbf{x}_U$ are coupled, because the sky coverage is symmetric about the north-south axis. For the case of $\theta_{\min} = 15^\circ$ and $\phi_c = 40^\circ$, we obtain

$$\Delta \mathbf{x}_E = -5.1G_E, \quad (\text{A16})$$

$$\Delta \mathbf{x}_N = -6.3G_N, \quad (\text{A17})$$

$$\Delta \mathbf{x}_U = 2.4G_N. \quad (\text{A18})$$

Hence, if the same magnitude of gradients for north and east component are imposed, the error in north component is about 20% larger than the east component. At the same time, the error in the vertical component appears because of the north-south asymmetry in GPS satellite distribution and the presence of G_N .

[32] **Acknowledgments.** We thank Yuki Hatanaka for making use of his antenna phase variation model to public. We also thank Koji Matsumoto for providing the ocean loading coefficients at GEONET stations. GPS data are provided by the Geographical Survey Institute, Japan. Critical reviews by T. A. Herring, D. S. MacMillan, and an anonymous reviewer significantly improved the quality of this manuscript. A software package, Generic Mapping Tool (GMT), was used to plot the figures. This study is granted by ‘‘GPS Meteorology Project in Japan,’’ grant 08640552, and grant 10559023 supported by Japanese Ministry of Education, Culture, Sports, Science and Technology.

References

- Bar-Sever, Y. E., P. M. Kroger, and J. A. Borjesson, Estimating horizontal gradients of tropospheric path delay with a single GPS receiver, *J. Geophys. Res.*, *103*, 5019–5035, 1998.
- Beutler, G., I. Bauersima, W. Gurtner, M. Rothacher, T. Schildknecht, and A. Geiger, Atmospheric refraction and other important biases in GPS carrier phase observations, *Monograph*, *12*, Sch. of Surv., Univ. of N. S. W., Kensington, Australia, 1988.
- Chen, G., and T. A. Herring, Effects of atmospheric azimuthal asymmetry on the analysis of space geodetic data, *J. Geophys. Res.*, *102*, 20,489–20,502, 1997.
- Davis, J. L., G. Elgered, A. E. Niell, and C. E. Kuehn, Ground-based measurement of gradients in the ‘‘wet’’ radio refractivity of air, *Radio Sci.*, *28*, 1003–1018, 1993.
- Hatanaka, Y., M. Sawada, A. Horita, and M. Kusaka, Calibration of antenna-radome and monument-multipath effect of GEONET-part 1: Measurement of phase characteristics, *Earth Planets Space*, *53*, 13–21, 2001a.
- Hatanaka, Y., M. Sawada, A. Horita, M. Kusaka, J. M. Johnson, and C. Rocken, Calibration of antenna-radome and monument-multipath effect of GEONET-part 2: Evaluation of the phase map by GEONET data, *Earth Planets Space*, *53*, 23–30, 2001b.

- Hatanaka, Y., T. Iizuka, M. Sawada, A. Yamagiwa, Y. Kikuta, J. M. Johnson, C. Rocken, Improvement of the analysis strategy of GEONET, *Bull. Geogr. Surv. Inst.*, *49*, 11–38, 2003.
- Heki, K., S. Miyazaki, and H. Tsuji, Silent fault slip following an interplate thrust earthquake at the Japan Trench, *Nature*, *386*, 595–598, 1997.
- Herring, T. A., Modelling atmospheric delays in the analysis of space geodetic data, in *Symposium on Refraction of Transatmospheric Signals in Geodesy*, *Neth. Geod. Commis. Ser.*, vol. 36, edited by J. C. DeMunk and T. A. Spoelstra, pp. 157–164, Ned. Comm. Voor Geod., Delft, 1992.
- Iwabuchi, T., I. Naito, and N. Mannoji, A comparison of Global Positioning System retrieved precipitable water vapor with the numerical weather prediction analysis data over the Japanese Islands, *J. Geophys. Res.*, *105*, 4573–4585, 2000.
- Iwabuchi, T., S. Miyazaki, K. Heki, I. Naito, and Y. Hatanaka, An impact of estimating tropospheric delay gradients on tropospheric delays estimations in the summer using the Japanese nationwide GPS array, *J. Geophys. Res.*, *108*(D10), 4315, doi:10.1029/2002JD002214, 2003.
- Kato, N., and T. Hirasawa, A model for possible crustal deformation prior to a coming large interplate earthquake in the Tokai district, central Japan, *Bull. Seismol. Soc. Am.*, *89*, 1401–1417, 1999.
- MacMillan, D. S., Atmospheric gradients from very long baseline interferometry observations, *Geophys. Res. Lett.*, *22*, 1041–1044, 1995.
- Matsumoto, K., T. Sato, T. Takanezawa, and M. Ooe, GOTIC2: A program for computation of oceanic tidal loading effect, *J. Soc. Jpn.*, *47*, 243–248, 2001.
- Miyazaki, S., H. Tsuji, Y. Hatanaka, Y. Abe, A. Yoshimura, K. Kamada, K. Kobayashi, H. Morishita, and Y. Iimura, Establishment of the nationwide GPS array (GRAPES) and its initial results on the crustal deformation of Japan, *Bull. Geogr. Surv. Inst.*, *42*, 27–41, 1996.
- Miyazaki, S., T. Saito, M. Sasaki, Y. Hatanaka, and Y. Iimura, Expansion of GSI’s nationwide GPS array, *Bull. Geogr. Surv. Inst.*, *43*, 23–34, 1997.
- Naito, I., Y. Hatanaka, N. Mannoji, R. Ichikawa, S. Shimada, T. Yabuki, H. Tsuji, and T. Tanaka, Global Positioning System project to improve Japanese weather, earthquake predictions, *Eos Trans. AGU*, *79*, 301, 308, 311, 1998.
- Niell, A. E., Global mapping functions for the atmospheric delay at radio wavelength, *J. Geophys. Res.*, *101*, 3227–3246, 1996.
- Rocken, C., R. Ware, T. Van Hove, F. Solheim, C. Alber, J. Johnson, M. Bevis, and S. Businger, Sensing atmospheric water vapor with the Global Positioning System, *Geophys. Res. Lett.*, *20*, 2631–2634, 1993.
- Rothacher, M., and L. Marvert, *Bernese GPS Software Version 4.0*, Univ. of Berne, Berne, Switzerland, 1996.
- Saastamoinen, J., Atmospheric correction for the troposphere and stratosphere in radio ranging of satellites, in *The Use of Artificial Satellites for Geodesy*, *Geophys. Monogr. Ser.*, vol. 15, edited by S. W. Henriksen et al., pp. 247–251, AGU, Washington, D. C., 1972.
- Sagiya, T., A. Yoshimura, E. Iwata, K. Abe, I. Kimura, K. Uemura, and T. Tada, Establishment of permanent GPS observation network and crustal deformation monitoring in the southern Kanto and Tokai areas, *Bull. Geogr. Surv. Inst.*, *41*, 105–118, 1995.
- Santerre, R., Impact of GPS satellite sky distribution, *Manuser. Geod.*, *16*, 28–53, 1991.
- Shimada, S., H. Seko, H. Nakamura, K. Aonashi, and T. A. Herring, The impact of atmospheric mountain lee waves on systematic geodetic errors observed using the Global Positioning System, *Earth Planet Space*, *54*, 425–430, 2002.
- Tsuda, T., et al., GPS meteorology project of Japan—Exploring frontiers of geodesy, *Earth Planets Space*, *50*, i–v, 1998.
- Wdowinski, S., Y. Bock, J. Zhang, P. Fang, and J. Genrich, Southern California Permanent GPS Geodetic Array: Spatial filtering of daily positions for estimating coseismic and postseismic displacements induced by the 1992 Landers earthquake, *J. Geophys. Res.*, *102*, 18,057–18,070, 1997.
- Zumberge, J. F., M. B. Heflin, D. C. Jefferson, M. M. Watkins, and F. H. Webb, Precise point positioning for the efficient and robust analysis of GPS data from large networks, *J. Geophys. Res.*, *102*, 5005–5017, 1997.
- K. Heki, Division of Earth Rotation, National Astronomical Observatory, 2-12 Hoshigaoka, Mizusawa-city, Iwate 023-0861, Japan. (heki@miz.nao.ac.jp)
- T. Iwabuchi, Meteorological Research Institute, Japan Meteorological Agency, Nagamine 1-1, Tsukuba, Ibaraki, Tokyo 305-0052, Japan. (tiwabuch@mri-jma.go.jp)
- S. Miyazaki, Earthquake Research Institute, University of Tokyo, 1-1, Yayoi 1, Bunkyo-ku, Tokyo, 113-0032, Japan. (miyazaki@eri.u-tokyo.ac.jp)
- I. Naito, Division of Earth Rotation, National Astronomical Observatory, Mitaka, Tokyo 181-8588, Japan. (naito.isao@nao.ac.jp)